A computer simulation of local amorphization in III-V compounds

1993 J. Phys.: Condens. Matter 5 7907

(http://iopscience.iop.org/0953-8984/5/43/004)

J. Phys.: Condens. Matter 5 (1993) 7907–7922. Printed in the UK

A computer simulation of local amorphization in III–V compounds

I Jenčič†, J Peternelj† and I M Robertson‡

† Institut Jožef Stefan, Jamova 39, 61000 Ljubljana, Slovenia

‡ Department of Materials Science and Engineering, University of Illinois, Urbana, IL 61801, USA

Received 19 February 1993

Abstract. The formation of amorphous zones, induced by heavy-ion irradiation of III–V compounds and their ternary alloys, was studied using a computer simulation. For this purpose, the so-called sillium model, which has been used to model amorphous Si and Ge, was modified and subsequently employed in III–V compounds. The modification had to take into account different boundary conditions and different interatomic potentials in order to account for the partly ionic character of the bonds in these solids. For the Coulomb part of the potential we assumed rigid point ions with charges equal to the transversal effective charge. The results of the simulation show that the model is capable of producing a locally disordered structure surrounded by a perfect crystal lattice, provided that the energy of the initial displacement cascade is sufficiently high. It is also shown that the virtual crystal approximation is not adequate to confirm the experimentally observed differences in amorphization between GaAs and $Al_{0.85}Ga_{0.15}As$.

1. Introduction

Radiation damage in semiconductors results primarily in amorphization, which is a consequence of the highly directional character of covalent bonds. There are two distinct mechanisms responsible for the onset of amorphization. One prevails at light-ion irradiations where the concentration of point defects and the energy density in an individual displacement cascade are not high enough for a crystalline to amorphous (c–a) phase transition. With increasing ion dose, however, the overall concentration of point defects in the irradiated region can reach the point of the c–a transition. This is known as the *point-defect build-up* mechanism. On the other hand, heavy ions (with their mass comparable to the mass of atoms in the solid) produce highly concentrated displacement cascades and the material is amorphized locally, around the path of individual ions. The result is creation of a small ($\sim$ 3 nm in diameter) amorphous zone. This mechanism is called *direct-impact amorphization*.

The ternary alloy $Al_xGa_{1-x}As$ is, together with GaAs, very important for the production of heterostructures. In experimental research into the response of both materials to irradiation with heavy ions we have found [1, 2] that $Al_xGa_{1-x}As$ is much more resistant to amorphization than GaAs, and that this resistance increases with increased Al content. In particular, it has been shown that under all conditions of irradiation there was no evidence of direct-impact amorphization in an $Al_xGa_{1-x}As$ alloy with high Al content ($x = 85\%$). This peculiar result has motivated the present study.

0953-8984/93/437907+16$07.50

It is already clear that the increased resistivity of $Al_xGa_{1-x}As$, with high Al content, to amorphization cannot be attributed to a lower energy density† of the collision cascade in $Al_{0.85}Ga_{0.15}As$ than in GaAs (Al is a significantly lighter atom than Ga and the energy transfer during a single collision is smaller) for two reasons.

(1) Kr^+ ions produce direct-impact amorphization in GaAs [4, 5] and the cascade energy density for this case can be compared to the energy density of cascades of Xe^+ ions in $Al_{0.85}Ga_{0.15}As$. Xe^+ ions are heavier then Kr^+ ions, and therefore slower at the same kinetic energy. Hence, they have a shorter range and the density of energy deposition is relatively higher.

(2) Direct-impact amorphization is also observed in 50 keV Kr^+ irradiation of GaP [6], which has atomic masses very similar to those of AlAs.

Another possible explanation for the increased resistivity to amorphization would be that direct-impact amorphization in $Al_xGa_{1-x}As$ does occur, but the amorphous zones are subsequently rapidly recrystallized. Since no direct-impact amorphization has been observed even at 30 K, this explanation also seems to be ruled out. We are thus led to conclude that the structure and/or stability of the amorphous state in $Al_xGa_{1-x}As$ is significantly different from a similar condition in GaAs (and other 'common' III–V semiconductors).

To investigate the above hypothesis we have studied, using computer simulation, the structure of individual amorphous zones in III–V semiconductors. Amorphization is a complex phenomenon and is still far from being well understood. Consequently, we shall assume, in what follows, that the structure of the amorphous zones is not just a crystalline state containing a high density of vacancies, divacancies, interstitials, diinterstitials etc, but is pictured as a tetrahedral glass derived from the zincblende structure by topological disorder. Therefore we expect fairly sharp interfaces in a partially amorphous material separating regions that have relaxed to an amorphous phase from those that have not. A model of this kind, which has gained wide acceptance, is the so-called *continuous-random-network model* [7]. In this model every atom is almost perfectly tetrahedrally coordinated with its nearest neighbours. Distortions of bond lengths and bond angles from the values in the crystalline phase are of the order of 10%. Although the structure of the amorphous zones lacks the long-range crystalline order, the bond orbitals may still be visualized as directed hybridized orbitals of the familiar sp^3 type. This circumstance will be accounted for by an appropriate choice of the interatomic potential corresponding to short-range forces.

2. The sillium model and its application to modelling of amorphous zones

The algorithm for modelling of amorphization was adopted from the so-called *sillium model* [8], which is based on bond switching between two pairs of suitably chosen atoms (preserving the fourfold coordination), simulation of thermal relaxation using the Metropolis algorithm [9], and the use of the Keating potential [10] for the calculation of inter-atomic forces. In its original formulation the sillium model was used for construction of an infinite amorphous structure of a tetrahedrally bonded monoatomic solid, such as Si or Ge. The resulting radial distribution (RDF) compared favourably with the experimentally determined RDF of amorphous Ge, provided that the annealing process is performed carefully [8].

In spite of its deficiencies and limitations, in particular the use of a rather simple semiempirical interatomic potential, the sillium model nevertheless offers a useful method

† It is a very plausible assumption that a critical energy density must be reached before the material is rendered amorphous [3].

for constructing and categorizing realistic random networks. It is also true that its application to modelling of amorphous zones with their concomitant amorphous-crystal interfaces will perhaps further amplify the known deficiencies of the model. Considering the experimental results discussed above, however, it may still be of some interest to examine the structure of the resulting amorphous zones.

The actual rules determining the model are essentially those of Wooten and Weaire [8] and we list them for the sake of completeness.

(1) Every atom is bonded to four neighbours.

(2) In the process of randomization (or relaxation) the switching of bonds takes place, i.e. the bonds between two pairs of atoms are broken and a new pair of bonds is subsequently formed, between the same four atoms, but with the different atom pairs in each bond ('bond transposition').

(3) After a bond transposition, the atoms move to the equilibrium position (geometric relaxation), i.e., to the position with minimal potential energy as represented by the interatomic potential. Thermal vibrations are neglected.

(4) When a highly excited state is created via this initial randomization, an annealing process is simulated. Here, the allowed bond switches must satisfy the condition

$$w < \exp(-\Delta V/k_B T) \tag{1}$$

where w is a random variable between zero and unity, taken at each bond switch, ΔV is the difference of potential energy between the atomic configurations before and after the bond transposition, k_B is the Boltzmann constant and T the simulated temperature of annealing.

(5) Instead of the periodic boundary conditions used in [8], in our case the atoms are fixed at the edge of the amorphous region in the positions of the ideal crystal structure. Therefore, bond switches and movements of atoms are allowed only in the central region of the amorphous sphere. This region is surrounded with a shell of atoms where only movements of the atoms are allowed, thus enabling a smooth distribution of stresses along the amorphous crystalline interface. At the very edge, as we have already mentioned, the atoms are completely rigid and fixed in the positions of a perfect lattice. While for the sillium case, with the use of periodic boundary conditions, a model containing 216 atoms was adequate, our model requires at least a few thousands of atoms in order to yield an amorphous structure.

It is to be understood that in III–V compounds and their ternary alloys we have, in general, two or three different atoms participating in bond formations which are, as a consequence, partly ionic. This aspect must be accounted for by an appropriate choice of the interatomic potential, which also includes the determination of the effective charges associated with the atoms. We will address this problem in the next section.

3. The interatomic potential

The potential energy V of the system under consideration, corresponding to a non-equilibrium configuration $\{u_{1s}, u_{2s}, \ldots\} \equiv \{u\}$ of the atoms, is usually written as

$$V(\{u\}) = V(\{0\}) + \sum_{is} \frac{\partial V}{\partial u_{is}} \cdot u_{is} + \frac{1}{2} \sum_{is} \sum_{js'} u_{is} \cdot \frac{\partial^2 V}{\partial u_{is} \partial u_{js'}} \cdot u_{js'} + \cdots . \tag{2}$$

The radius vector $\boldsymbol{R}_{is}$ of the sth atom in the ith unit cell is assumed to have the form

$$\boldsymbol{R}_{is} = \boldsymbol{R}_{is}^{(0)} + \boldsymbol{u}_{is} \tag{3}$$

where $\boldsymbol{u}_{is}$ represents the displacement of the atom from its equilibrium position $\boldsymbol{R}_{is}^{(0)}$ in the crystal lattice. All $\partial V/\partial \boldsymbol{u}_{is}$ vanish, since they are evaluated at the equilibrium position $\boldsymbol{R}_{is}^{(0)}$. The coefficients

$$\partial^2 V/\partial u_{is}^{(\alpha)} \partial u_{js'}^{(\beta)}|_{\alpha,\beta\in(x,y,z)}$$

are the atomic *force constants*. Many are related by symmetry, but there are a number (of the order of the number of atoms in the crystal) that are independent and they must be known, if one wishes to calculate $\Delta V = V(\{u'\}) - V(\{u''\})$, using equation (2). We can determine some of the atomic force constants from the frequency measurements. However, a solid has many more force constants than frequencies, and thus no unique assignment of force constants can be obtained on the basis of frequency measurements alone [11].

It is possible, in principle, to calculate all the force constants from the theory of electronic structure. In covalent solids this proves to be extremely difficult in practice, even within the framework of the *bond orbital approximation* [12], which is especially suitable for the study of alloys and amorphous semiconductors [13]. The more practical alternative is to model interactions on the basis of theoretical ideas in order to reduce the number of independent force constants. Of the many force-constant models, perhaps the most useful description of the short-range forces in tetrahedrally coordinated solids is the so-called *valence-force-field* approach [14]. It is characteristic of all such models that the more constants one introduces, the more experimental constants one can fit.

In elemental semiconductors, such as Si and Ge, the interatomic forces can be resolved, quite accurately, into bond-stretching and bond-bending forces [10, 14]. The equations of motion as written in terms of the bond-stretching force constant α and bond-bending force constant β can be then compared, in the long wavelength limit, with the equation of motion resulting from macroscopic elasticity theory. In the case of crystals with cubic symmetry there are three independent macroscopic elastic constants c_{11}, c_{12} and c_{44} which are thus related to α and β. Using the experimental values for the elastic constants we can determine the magnitudes of α and β.

It is well known [15, 16] that the calculation of the elastic constants and their relation to atomic force constants is more demanding in the case of heteropolar semiconductors, such as GaAs and AlAs, for example, and their ternary alloys. In particular, one has to introduce explicitly the polarization of the crystal produced by the displacement and polarizability of the ion cores and the redistribution of the valence charge density.

The relation between the elastic constants c_{11}, c_{12} and c_{44} and the bond-stretching force constant α and the bond-bending force constant β, for the ZnS-type semiconductors, was derived by Martin [17]. He used the rigid point-ion approximation and a single effective charge Z^*e_0 defined by the optic-mode splitting in the long-wavelength limit [18]. We will use his results to determine the magnitude of α and β for GaAs, AlAs and $Al_xGa_{1-x}As$ from the known values of the elastic constants for these solids.

Adopting the results of Keating [10] and Martin [17], including the rigid point-ion approximation, we can write the interatomic potential corresponding to heteropolar tetrahedrally bonded crystalline semiconductors, containing a single amorphous zone, as

$$V = \frac{1}{2}\sum_i \left[\frac{2\alpha}{a_0^2}\sum_{i=1}^{4}(r_{li}^2 - d_0^2)^2 + \frac{4\beta}{a_0^2}\sum_{i,j>i}\left(\boldsymbol{r}_{li}\cdot\boldsymbol{r}_{lj} + \frac{1}{3}d_0^2\right)^2\right.$$

$$-\sum_{i=1}^{4}\frac{1}{4}\alpha_M\frac{(Z^*e_0)^2}{4\pi\epsilon_1\epsilon_0 d_0^2}(r_{li}-d_0)-\frac{\alpha_M(Z^*e_0)^2}{4\pi\epsilon_1\epsilon_0 d_0}\Bigg]+\Delta V_{AZ} \tag{4}$$

where the index $l \equiv (i,s)$ runs over all the atoms, r_{li} is the vector pointing from atom l to its nearest neighbour i, a_0 is the lattice constant and $d_0 = \frac{1}{4}a_0\sqrt{3}$, is the equilibrium bond length. Z^*e_0 will be assumed to be equal to the transversal effective charge $e_T^*e_0$ [17, 18], α_M is the Madelung constant, and ϵ_0 and ϵ_1 are the permittivity of free space and the electronic dielectric constant, respectively. We should point out, however that in general $\alpha = \alpha(l,i)$ and $\beta = \beta(l,i,j)$. ΔV_{AZ} is the change in the electrostatic potential due to the presence of the amorphous region embedded in the crystal lattice. To obtain an approximate expression for ΔV_{AZ} we make use of the following rather trivial observation. When an ionic charge Z^*e_0 is displaced by $\boldsymbol{u}$, the net effect is as though a charge $-Z^*e_0$ has been placed at the undisplaced position of the ion and a fresh charge Z^*e_0 has been created at the displaced position. The displacement, if it is not too large, is equivalent to the addition of a dipole moment with the moment $Z^*e_0\boldsymbol{u}$. It then follows that

$$\begin{aligned}\Delta V_{AZ} = &-\frac{1}{2}\alpha_M\frac{(Z^*e_0)^2}{4\pi\epsilon_1\epsilon_0 d_0}\sum_{l\in AZ}\left(\frac{q_l'}{q_l}-1\right)-\sum_{l\in AZ}\left(\frac{q_l'}{q_l}\right)(\boldsymbol{u}_l\cdot\nabla_{\boldsymbol{R}_l^{(0)}})F(\boldsymbol{R}_l^{(0)})\\
&+\frac{1}{2}\sum_{\substack{l,l'\in AZ\\ l\neq l'}}\Bigg(\frac{(q_l'-q_l)(q_{l'}'-q_{l'})}{4\pi\epsilon_1\epsilon_0 R_{ll'}^{(0)}}\\
&+q_l'(q_{l'}'-q_{l'})\frac{\boldsymbol{u}_l\cdot\boldsymbol{R}_{ll'}^{(0)}}{4\pi\epsilon_1\epsilon_0 R_{ll'}^{(0)3}}-q_{l'}'(q_l'-q_l)\frac{\boldsymbol{u}_{l'}\cdot\boldsymbol{R}_{ll'}^{(0)}}{4\pi\epsilon_1\epsilon_0 R_{ll'}^{(0)3}}\\
&+\frac{q_l'q_{l'}'}{4\pi\epsilon_1\epsilon_0 R_{ll'}^{(0)5}}[R_{ll'}^{(0)2}\boldsymbol{u}_l\cdot\boldsymbol{u}_{l'}-3(\boldsymbol{u}_l\cdot\boldsymbol{R}_{ll'}^{(0)})(\boldsymbol{u}_{l'}\cdot\boldsymbol{R}_{ll'}^{(0)})]\Bigg)\end{aligned} \tag{5}$$

where $F(\boldsymbol{R}_l^{(0)})$ is proportional to the Ewald expression for the Madelung constant written in the rapidly convergent form [15, 16]

$$\begin{aligned}F(\boldsymbol{R}_{is}^{(0)}) = &-\frac{3\sqrt{3}}{128E^2\epsilon_1\epsilon_0}\sum_{s'}q_{is}q_{is'}\sum_{\boldsymbol{G}\neq 0}\frac{\exp(-d_0^2G^2/4E^2)}{d_0^2G^2/4E^2}\exp[-i\boldsymbol{G}(\boldsymbol{R}_{i's'}^{(0)}-\boldsymbol{R}_{is}^{(0)})]\\
&-\frac{E}{8\pi\epsilon_1\epsilon_0}\sum_{i's'\neq is}q_{is}q_{i's'}H(E|\boldsymbol{R}_{i's'}^{(0)}-\boldsymbol{R}_{is}^{(0)}|/d_0)+\frac{E}{\sqrt{\pi}}\frac{q_{is}^2}{4\pi\epsilon_1\epsilon_0}\end{aligned} \tag{6}$$

and the function $H(x)$ is defined as

$$H(x) = \frac{2}{\sqrt{\pi}}\frac{1}{x}\int_x^\infty ds\exp(-s^2).$$

$\boldsymbol{G}$ is a vector of the reciprocal lattice and E is a number of the order of unity, chosen in such a way as to lead to the rapid convergence of both sums in (6). $q_l = \pm Z^*e_0$ is the ionic charge at the site $l \equiv (i,s)$ in a perfect crystal lattice, while q_l' is the corresponding charge in a disordered lattice and is, in general, different from q_l if l belongs to the amorphous zone ($l \in AZ$). $R_{ll'}^{(0)} \equiv |\boldsymbol{R}_l^{(0)} - \boldsymbol{R}_{l'}^{(0)}|$.

Using the experimental results quoted in [17] and [19] we calculated the parameters appearing in (4) and (5). Their values are listed in table 1 for several III–V compounds.

Table 1. Parameters of the Martin potential of selected III–V compounds [17, 19]. a_0 is the lattice constant, and $d_0 = \frac{1}{4}a_0\sqrt{3}$ is the equilibrium bond length; e_T^* is the transversal effective charge (in units of e_0) and ϵ_1 is the electronic dielectric constant; α and β are the bond-stretching and bond-bending force constants, respectively; and α_M is the Madelung constant.

Compound	a_0 (nm)	e_T^{*2}/ϵ_1	α (eV nm^{-2})	β (eV nm^{-2})	αa_0^2 (eV)	$\alpha_M e_T^{*2} e_0^2/4\pi\epsilon_1\epsilon_0 d_0$ (eV)
Si	*0.5431*	—	302.81	86.19	89.31	0.00
Ge	0.5658	—	241.65	71.07	77.35	0.00
GaAs	0.5653	0.444	259.55	56.01	82.95	4.39
$Al_{0.85}Ga_{0.15}As$	0.5660	0.511	269.91	54.53	86.47	5.05
AlAs	0.5661	0.588	273.57	54.07	87.67	5.82
GaP	0.5451	0.494	294.92	65.28	87.62	5.07

To calculate the corresponding values for the ternary alloy $Al_xGa_{1-x}As$, we employed the so-called *virtual-crystal approximation* [20], where, for example

$$\alpha_{Al_xGa_{1-x}As} = x\alpha_{AlAs} + (1-x)\alpha_{GaAs}.$$

This may not seem a very good approach to the problem at hand, however, we believe it is nevertheless a useful zero-order approximation, which simplifies the calculations considerably. Also, if we neglect the terms quadratic in the atomic displacements u_l, (5) can be further simplified to yield:

$$V - V_{\text{Madelung}} = \alpha a_0^2 \sum_l \left\{ \sum_{i=1}^{4} \left(\frac{r_{li}^2}{a_0^2} - \frac{3}{16} \right)^2 + 2\frac{\beta}{\alpha} \sum_{i,j>i} \left(\frac{\boldsymbol{r}_{li} \cdot \boldsymbol{r}_{lj}}{a_0^2} + \frac{1}{16} \right)^2 + \frac{\frac{2}{3}\alpha_M e_T^{*2} e_0^2/4\pi\epsilon_1\epsilon_0 a_0}{\alpha a_0^2} \sum_{i=1}^{4} \left[\frac{\sqrt{3}}{4}(1 + \xi_l'\xi_i') - (1 + \kappa\xi_l'\xi_i') \left(\frac{r_{li}}{a_0} - \frac{\sqrt{3}}{4} \right) \right] \right\} \tag{7}$$

where $q_l' = e_T^* e_0 \xi_l'$, $\xi_l' = \pm 1$, and the influence of antisite disorder at the higher-order neighbours has been neglected. κ is a constant and is equal to 1.26. Using the results given in table 1, one can see that the contribution of the Coulomb interactions to the total potential V is rather small ($\sim 6\%$) in comparison to the short-range Keating potential. It may thus appear that the specific choice of the effective charge $Z^* e_0 = e_T^* e_0$ is not very crucial.

It is clear that in solids there are essential ambiguities in associating effective charges with ions. Fortunately there are experimentally distinguishable configurations of the lattice that lead to the natural definitions of the effective charges associated with each type of lattice distortion (piezoelectric effect, the splitting of longitudinal and transverse optical modes of lattice vibrations in the zincblende structure). Rather than going into a detailed discussion of the proper definition of the effective charge corresponding to each case [21–24], we follow Martin [17] and use a single effective charge given by

$$(Z^* e_0)^2 \equiv (e_T^* e_0)^2 = \tfrac{1}{4}\mu a_0^3 \epsilon_0 \epsilon_1 [\omega_{LO}^2 - \omega_{TO}^2] \tag{8}$$

where ϵ_1 is the electronic dielectric constant, a_0 is the lattice constant, μ is the reduced mass of the two atoms in a primitive unit cell and ω_{LO} and ω_{TO} are the long-wavelength longitudinal and transverse optical mode frequencies, respectively. The numerical values of e_T^{*2}/ϵ_1 are given in table 1.

Table 2. Parameters of a thermal spike. T_m is the melting temperature, λ is the thermal conductivity, Θ_D is the Debye temperature, E_d is the displacement energy and t_0 is the atomic vibration period. The parameters t_m, r_m and n_m are calculated for a spike with $E = 5$ keV and are characteristic values of thermal-spike melting time, radius and the number of atoms, respectively, as defined in section 4.

	GaAs	$Al_{0.85}Ga_{0.15}As$
T_m (K)	1511	1866
λ (W mK^{-1})	44.05	19.61
Θ_D (K)	370	432
E_d (eV)	17	17
t_0 (ps)	0.130	0.111
t_m (ps)	0.157	0.379
r_m (nm)	2.12	1.98
n_m (atoms)	1778	1439

4. The parameters of randomization and relaxation calculation

Due to computer limitations a 5 keV displacement cascade was simulated. At the initial randomization, the temperature T of the cost function (1) is, as in the sillium model, quite arbitrary, and the initial temperature was chosen such that $k_BT = 20$ eV. This energy is comparable with both the displacement energy in GaAs, which is 17 eV [25], and the initial core energy of a thermal spike (table 3). Besides, an energy equal to 20 eV enables up to three different bond transpositions from the initial, perfect crystal structure. In the process of the initial randomization, bond transpositions were allowed inside a sphere which contained $n_{trans} = (5000 \text{ eV})/(20 \text{ eV}) = 250$ atoms. On the average, one bond transposition attempt per atom was made and each such attempt had to satisfy the following criteria.

- Before the transposition the distance between the atoms of both bonds was smaller than 0.8 of the lattice constant a_0, i.e., smaller than 1.85 of the equilibrium interatomic distance d_0—this is a slightly larger distance than the distance between the next-nearest neighbours in a perfect diamond structure; if the maximal allowed distance were smaller than $0.71a_0$, the starting randomization would not be possible.
- Bond transposition is topologically possible, i.e., after the transposition no double bonds were formed.
- The transpositions where three- or fourfold bond rings would be formed were not allowed.

This structure, formed in the transposition volume, was subsequently relaxed; in addition to the atoms in the randomized sphere, relaxation was also allowed in a shell around this sphere, and this shell contained at least two atomic layers. Such a shell is sufficiently thick that after the relaxation the stresses on the outer edge of the 'relaxed' shell are negligible.

For the simulation of annealing the *thermal-spike* model [26] was used. This model is based on the assumption that the energy transferred to the lattice by the incident ion is localized in a very small volume. Consequently the high energy concentration causes local melting. In the melted region, the atomic migration and recombination is very intensive, followed by a fast cool down and 'freezing' of the atoms in a disordered structure.

The practical validity of this model depends on volume and time to which the macroscopic concepts of heat can be applied. In insulators and semiconductors these limits are determined by the frequencies of atomic vibrations (10^{12}–10^{13} s^{-1}) and the mean free path of phonons (1–5 nm at room temperature). Consequently, it would be unsafe to apply the macroscopic concept of heat for times shorter than 10^{-12} s and volumes with linear

dimensions much less than 5 nm. However, it has been shown [27], using the *molecular-dynamics* method that a process similar to melting does take place in the displacement spike, and that this process is responsible for the intensive mixing of the atoms. Having this in mind, one can therefore justify the use of idealized thermal-spike equations to obtain an estimate for the order of magnitude of the temperature and the size of the spike.

Approximating the initial energy distribution by $E\delta(r)$, where $\delta(r)$ is the Dirac delta function, the solution of the diffusion equation yields the following temperature at time t:

$$T = \frac{E}{\rho c_p} \frac{\exp(-r^2/4Dt)}{(4\pi Dt)^{3/2}}. \tag{9}$$

Here $D = \lambda/\rho c_p$ is the diffusion coefficient, λ the heat conductivity, ρ the density, c_p the heat capacity of the material and r the distance from the origin.

The time at which the temperature reaches its maximal value at the radius r can be obtained by differentiating equation (9) with respect to t. The result is

$$t_r = r^2/6D. \tag{10}$$

The radius of the sphere within which the temperature exceeds a particular temperature T_m is therefore

$$r_m = \sqrt{\frac{3}{2\pi e}} \left(\frac{E}{\rho c_p T_m}\right)^{1/3}. \tag{11}$$

where e is the basis of natural logarithms. Now, the equation (9) can be written in a shortened form as

$$\mathcal{T} = \exp[\tfrac{3}{2}(1 - x^2/\tau)]/\tau^{3/2} \tag{12}$$

where we have introduced new, 'reduced' variables:

$$\mathcal{T} = T/T_m \tag{13}$$

$$x = r/r_m \tag{14}$$

$$\tau = t/t_m \equiv t/(r_m^2/6D). \tag{15}$$

The 'spike core' is defined as the region with radius $r_0 = \sqrt{6Dt}$, where the temperature is decreasing with time. Simple calculation shows that the average temperature of the spike core is

$$\langle \mathcal{T} \rangle_c = \frac{3}{x_0^3} \int_0^{x_0} \frac{\exp[\frac{3}{2}(1 - x^2/\tau)]}{\tau^{3/2}} x^2 \, dx \tag{16}$$

$$x_0 = \sqrt{\tau} \tag{17}$$

and after numerical integration one obtains

$$\langle \mathcal{T} \rangle_c = 1.973/\tau^{3/2}. \tag{18}$$

In the simulation of the annealing process, (17) and (18) were used for the determination of the transposition volume and annealing temperature, respectively. The radius of the spike core at time t is therefore equal to

$$r_{\text{trans}} = r_{\text{m}}\sqrt{t/t_{\text{m}}} \tag{19}$$

and the transposition volume is equal to

$$n_{\text{trans}} = n_{\text{m}}(t/t_{\text{m}})^{3/2} \tag{20}$$

where n_{m} is the maximal number of 'melted' atoms. The average temperature in the transposition volume can be obtained from equation (18) to be

$$T_{\text{trans}} \simeq 2T_{\text{m}}t_{\text{m}}^{3/2}/t^{3/2}. \tag{21}$$

Table 2 gives the values of the material parameters necessary to calculate r_{m} and t_{m}.

The time scale of annealing steps was determined by t_0, the typical period of atomic vibrations

$$t_0 = h/k_{\text{B}}\Theta_{\text{D}} \tag{22}$$

where h is Planck's constant and Θ_{D} the Debye temperature.

At a given temperature T, the probability for a successful bond transposition with $\Delta E \geqslant k_{\text{B}}T$ is equal to e^{-1}. Therefore, if the number of attempts in a selected time interval is en_{trans}, then, on average every atom would have a chance for a successful bond transposition with a potential difference of at least $k_{\text{B}}T$. Instead of this, the number of time intervals was multiplied by e, and the number of attempts was fixed at the value 1/atom. The time intervals, which were used to calculate the temperature T_{trans} and radius r_{trans} of the annealing steps, were therefore determined by the equation

$$t(k) = (k/\text{e})t_0 \qquad (k = 1, 2, 3, \ldots). \tag{23}$$

Table 3 gives the calculated values of the temperature and volume of the sphere at these time intervals for GaAs and $Al_{0.85}Ga_{0.15}As$; due to a lower thermal conductivity and higher melting point, the cooling time (and the number of annealing steps) in $Al_{0.85}Ga_{0.15}As$ is appreciably higher than that in GaAs.

When the spike core temperature drops below ~ 0.7 eV, the transposition volume was not expanded further in accordance with equation (20), but the former value was kept constant. This restriction was justified for the following reason: energetically the lowest transposition from the perfect crystal structure increases the potential energy by 7.7 eV in GaAs, and by 8.3 eV in $Al_{0.85}Ga_{0.15}As$. The probability for a successful transposition from a perfect crystal structure is therefore $\sim \exp(-8/0.7) \simeq 10^{-5}$ and with falling temperature this value decreases exponentially; the perfect structure is, of course, only in the outer, expanded part of the sphere and hence, at $k_{\text{B}}T < 0.7$ eV, the transpositions are practically impossible; this temperature, however, still enables transpositions in the central part of the sphere, since it is already in a disordered state and transpositions with smaller energy differences are possible. On the other hand, such a restriction has enabled rationalization in terms of computer time, and, in turn, made it possible to simulate a thermal spike with larger energy.

After the spike core temperature had fallen below the melting point, the room-temperature value for the thermal conductivity was used and the cooling process became several times faster than before. Since $k_B T$ is very small in comparison with the typical transposition energy, the temperature was assumed constant, at 300 K. The number of bond-switch attempts per atom was determined from the time required for cooling from the melting point to 30 K. Another 300 iterations per atom followed at 30 K; at this temperature, practically only transpositions with a negative energy difference are possible and 300 iterations were made to ensure that all such transpositions had a fair chance (usually the last transposition was around the 100th iteration). Table 3 shows the simulation parameters at given iteration steps.

Table 3. The input for the simulation.

	GaAs			$Al_{0.85}Ga_{0.15}As$		
k	$k_B T_{trans}$ (eV)	n_{trans} (atoms)	n_{relax} (atoms)	$k_B T_{trans}$ (eV)	n_{trans} (atoms)	n_{relax} (atoms)
1	3.42	296	608	19.90	51	147
2	1.21	839	1461	7.04	144	337
3	0.66	1455	2353	3.83	265	553
4	0.43	1455	2353	2.49	408	793
5	0.31	1455	2353	1.78	570	1051
6	0.23	1455	2353	1.35	749	1326
7	0.18	1455	2353	1.07	944	1617
8	0.15	1455	2353	0.88	1153	1923
9	—	—	—	0.74	1376	2242
10	—	—	—	0.63	1455	2353
11	—	—	—	0.55	1455	2353
12	—	—	—	0.48	1455	2353
13	—	—	—	0.42	1455	2353
14	—	—	—	0.38	1455	2353
15	—	—	—	0.34	1455	2353
16	—	—	—	0.31	1455	2353
17	—	—	—	0.28	1455	2353
18	—	—	—	0.26	1455	2353
19	—	—	—	0.24	1455	2353
20	—	—	—	0.22	1455	2353
21	—	—	—	0.21	1455	2353
22	—	—	—	0.19	1455	2353
23	—	—	—	0.18	1455	2353
24	—	—	—	0.17	1455	2353
Number of iterations						
20	0.03	1455	2353	—	—	—
57	—	—	—	0.03	1455	2353
300	0.003	1455	2353	0.003	1455	2353

5. The results of simulation and discussion

The simulation was performed on the VAX/VMS computers (VAX 8650, μVAX-4000, μVAX-III). Since a probabilistic method is involved, several (i.e., six for GaAs and six for

$Al_{0.85}Ga_{0.15}As$) simulations were carried out with the same input data for each material. After the simulation was completed, each resulting structure was analysed.

As is well known, the absence of a sharp structure in the scattering pattern of an incident monoenergetic collimated beam of x-rays or particles is the principal experimental evidence that the material is amorphous. The simplest comparison between the models and the experiment is obtained with the help of the RDF, which we define as in [8], and which is denoted by

$$g(r) = 4\pi r^2 \rho(r).$$

$\rho(r)$ is the local density of atoms at a distance r from a particular atom averaged with the respect to the choice of this atom. However, for quantitative comparisons the closely related *correlation function*

$$t(r) = g(r)/r$$

is usually used. For example, the correlation function corresponding to a perfect diamond cubic structure shows a number of sharp peaks [8]. With increasing randomization the correlation function becomes more and more featureless, apart from the first and second peaks which are characteristic of tetrahedral bonding. The most notable difference between the correlation functions for crystalline and amorphous material is in the absence of the third peak, which is prominent in the crystalline phase.

An example of the structure resulting from our model of randomization is shown in figure 1, representing a cross-section through the (111) plane. The corresponding correlation functions, where an average over the first 200 central atoms was taken into account, are shown in figure 2. In all simulations, one bond transposition attempt per atom was made on the average inside the transposition volume. The number of successful bond transpositions per atom is denoted by c. It ranged from 0.39 to 0.46 for GaAs and from 0.32 to 0.42 for $Al_{0.85}Ga_{0.15}As$. In all cases the lowest and highest c values yielded crystalline and amorphous structure, respectively, upon annealing. However, at intermediate values of c there was no observable correlation between the c values and the resulting structure. On average, we may conclude that the 5 keV cascade produces amorphous structure in approximately half of the simulations (curve b in figure 2), while in the other half of the simulations the correlation function corresponding to the resulting structure (curve a in figure 2) retains a fair amount of structure characteristic of the crystalline state. Similar conclusions are also obtained from the bond-length and bond-angle distributions shown in figures 3 and 4, respectively. It is also seen from table 4 that the RMS bond-length and angular deviations from their mean values (which are essentially identical to the values corresponding to perfect tetrahedral bonding) are 5.7% and 20%, respectively. These values are roughly factors of three and two larger, respectively, than the corresponding experimental values obtained for amorphous Ge [28, 29].

Table 4. Average value and RMS deviation of bond lengths and bond angles.

	Bond length (a_0)	Angle between bonds
Perfect crystal	0.4330	109°28′
'Crystal + defects'	0.4348 ± 4.6%	109°16′ ± 16%
'Amorphous'	0.4332 ± 5.7%	108°24′ ± 20%

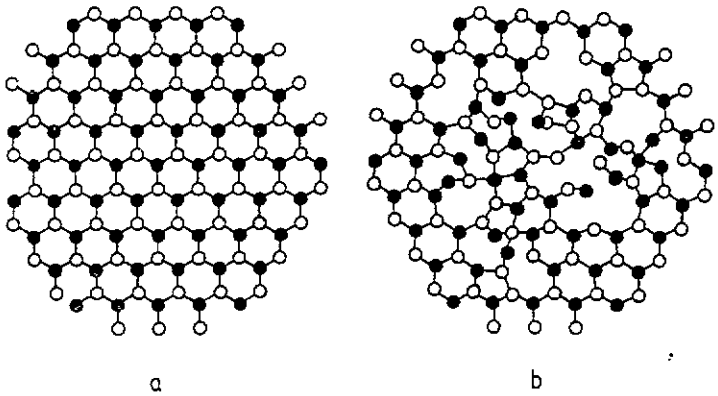

Figure 1. (111) plane: (a) a perfect zincblende lattice, (b) a deformed, 'amorphized' structure.

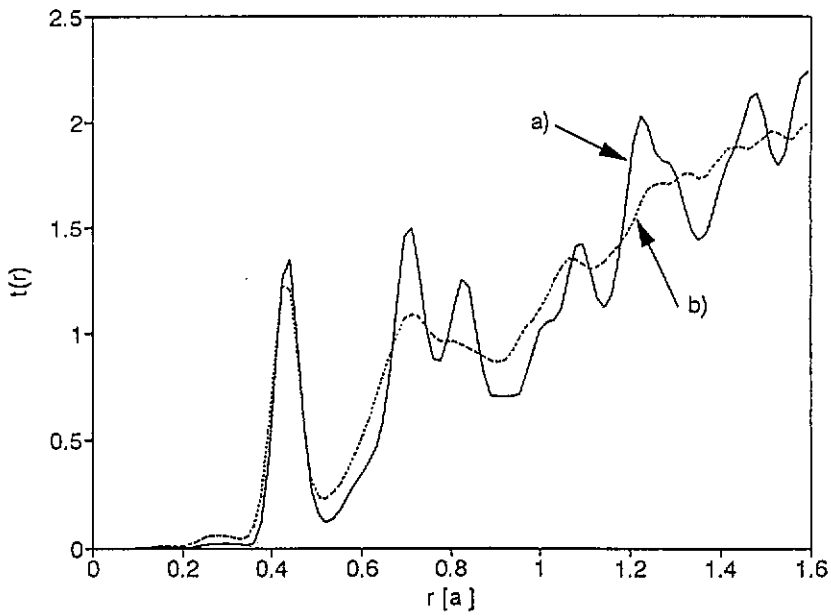

Figure 2. RDF for two simulations of GaAs and $Al_{0.85}Ga_{0.15}As$: (a) the presence of higher-order-neighbour peaks suggests a crystalline structure with some localized defects; (b) non-existence of higher-order-neighbour peaks suggests an amorphous structure.

As we have already mentioned, the contribution of the Coulomb part to the short-range potential is, in the approximation considered (equation (7)), around 6%. Consequently, the results of the simulation may be also compared with the corresponding results for Si and Ge obtained in [8] and applicable to type-IV semiconductors. It has been shown by Wooten and Weaire [8] that the initial randomization characterized by $c \simeq 0.3$ corresponds, apart from the first- and second-neighbour peaks, to a completely featureless correlation function, yet the subsequent annealing process leads back to the original diamond structure. In our case we have the initial randomization characterized by $0.32 \leqslant c \leqslant 0.46$, and the annealing process, governed by the thermal-spike model, almost restores the original crystalline state

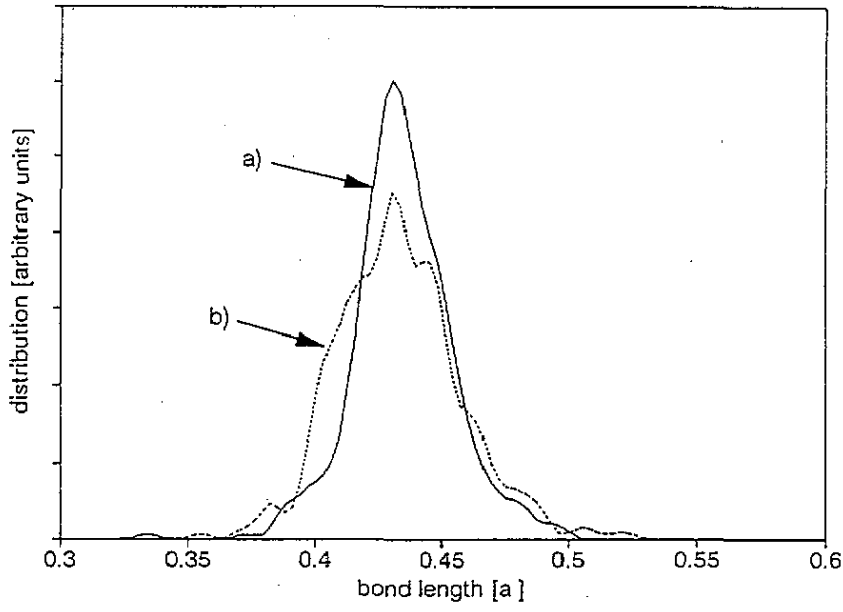

Figure 3. The distribution of bond lengths for two simulations: (a) structure with some crystalline order remaining; (b) amorphized structure.

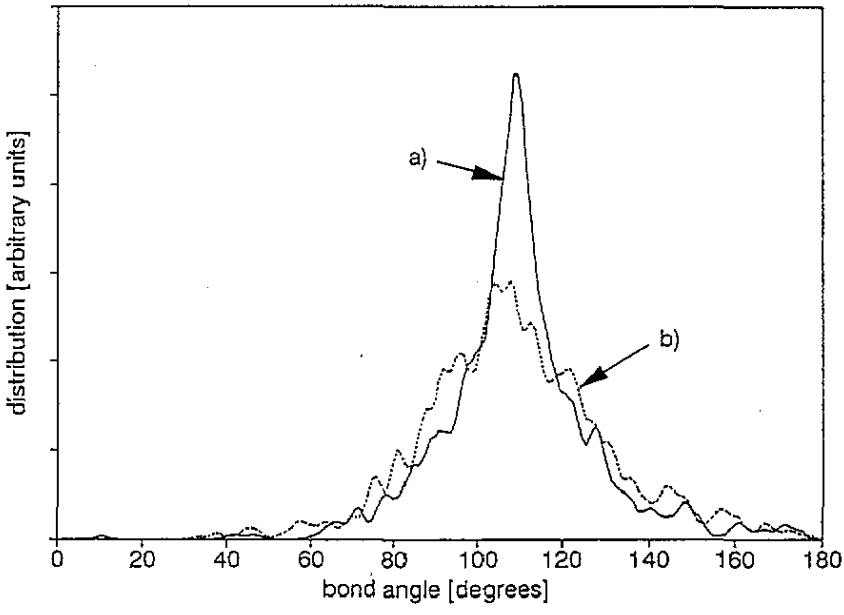

Figure 4. The distribution of bond angles for two simulations: (a) structure with some crystalline order remaining; (b) amorphized structure.

($c < 0.1$) in half of the cases, while in the other cases we obtain a random structure. At the

same time we can see from figure 2 and table 4 that the annealing process is less effective in reducing the bond and angular distortions when dealing with local amorphization compared to an infinite amorphous structure. In spite of this deficiency of the annealing process, which is also present to a lesser degree in the sillium model, we may conclude, in view of the above comparison, that a 5 keV displacement cascade is probably too small to generate sufficient initial randomization. This conclusion is strengthened even further when one considers the dependence of the structure factor $S(G)$ on the degree of initial randomization [30].

The results of the simulations have also shown that the Martin potential employed in this calculation is far too simple to account for the differences in behaviour of GaAs and $Al_{0.85}Ga_{0.15}As$ under irradiation. In this context we suggest two immediate modifications, which should improve the model. First of all, the virtual-crystal approximation is probably not adequate to bring out the difference between the behaviour of GaAs and $Al_xGa_{1-x}As$ under irradiation. In this approximation the parameters corresponding to GaAs and $Al_{0.85}Ga_{0.15}As$ differ only by about 10%. In future calculations one should distinguish between α_{Ga-As}, α_{Al-As}, $\beta_{As-Ga-As}$, $\beta_{Ga-As-Ga}$, $\beta_{As-Al-As}$, $\beta_{Al-As-Al}$ and $\beta_{Al-As-Ga}$, the values of which could perhaps be estimated with the use of bond-orbital approximation [12, 13]. Moreover the approximation (7) should be dropped and the expression (5) should be used for the calculation of Coulombic interaction.

On a more ambitious note, one could also dispose of the rigid-ion model itself. In the past various models have been proposed. Especially detailed analysis, also including III–V compounds, has been performed by Kunc and coworkers [31–33]. Their results can be incorporated into our calculation on the basis of the following observation. The displacements of the ions destroy the high symmetry of the corresponding lattice sites and lead to the appearance of the polarization of the crystal. We account for this by associating with each lattice site (this may prove ambiguous especially in the case of III–V compounds with partly ionic character of covalent bonds) a charge distribution characterized by multipole moments. Following Kunc *et al* [32, 33] we write the α-component of the dipole moment at the lattice site $l \equiv (i, s)$ as

$$p_l^{(\alpha)} = q_l' u_l^{(\alpha)} + \sum_{\beta,l'} m_{l,l'}^{(\alpha,\beta)} u_{l'}^{(\beta)} + \sum_{\beta,l'} \alpha_{l,l'}^{(\alpha,\beta)} E_{\text{eff}}^{(\beta)}(l'). \tag{24}$$

$q_l' = \pm q$ is the static ionic charge determined by fitting to the piezoelectric constant, $m_{l,l'}^{(\alpha,\beta)}$ are called mechanical polarizabilities or deformabilities, and $\alpha_{l,l'}^{(\alpha,\beta)}$ are the electronic polarizabilities representing the response of the electronic charge to the effective electric field. This field may be calculated for a given lattice site by the application of Ewald's method as described in [16]. However, in the case of a single amorphous zone, where the ionic displacements are limited to a localized region, we can solve the resulting equation by iteration and write in the first approximation

$$E_{\text{eff}}(l) = \sum_{\substack{l' \in AZ \\ l' \neq l}} (-q_l + q_l') \frac{\boldsymbol{R}_l^{(0)} - \boldsymbol{R}_{l'}^{(0)}}{4\pi\epsilon_0 R_{ll'}^{(0)3}} + \sum_{\substack{l' \in AZ \\ l' \neq l}} \left(q_l' \frac{3(\boldsymbol{R}_{ll'}^{(0)} \cdot \boldsymbol{u}_{l'})\boldsymbol{R}_{ll'}^{(0)} - R_{ll'}^{(0)2}\boldsymbol{u}_{l'}}{4\pi\epsilon_0 R_{ll'}^{(0)5}} \right) + \cdots \tag{25}$$

where l belongs, in general, to an arbitrary lattice site. Inserting (25) in (24) we obtain a reasonable approximation for the dipole moment associated with the lattice site l which can

be used then in (5) instead of $q_l' u_l$†. The transverse effective charge $e_T^* e_0$ can be expressed in terms of the high-frequency dielectric constant ϵ_1 and Szigeti effective charge q^*, which, in turn, can be written in terms of the static ionic charge q and the mechanical polarizabilities [32].

Extending the rigid-ion model in the manner indicated above inevitably brings new parameters into the model. Such parameters are usually determined by fitting to the available experimental data. Even if sufficient experimental data exist, such a procedure often proves very ambiguous and it is difficult to assign a clear physical meaning to all the parameters. This point has been emphasized very clearly already in [32] where it also has been demonstrated that when attempting to establish more sophisticated models, the results of simpler models may provide a very useful guide.

Acknowledgments

This research was supported by the Ministry of Science and Technology of Slovenia. IMR would like to acknowledge support from DOE, contract DEFG02-91-ER45439

References

[1] Jenčič I, Bench M W, Robertson I M and Kirk M A 1991 *J. Appl. Phys.* **69** 1287
[2] Jenčič I, Bench M W, Robertson I M, Kirk M A and Peternelj J 1991 *Nucl. Instrum. Methods* B **59/60** 458
[3] Thompson D A 1981 *Radiat. Eff.* **56** 105
[4] Vetrano J S, Bench M W, Robertson I M and Kirk M A 1989 *Metall. Trans.* A **20** 2673
[5] Bench M W, Robertson I M and Kirk M A 1988 *Mater. Res. Soc. Symp. Proc.* vol 100 (Pittsburgh, PA: Materials Research Group) p 293
[6] Bench M W, Robertson I M and Kirk M A 1991 *Nucl. Instrum. Methods* B **59/60** 372
[7] Zachariasen W H 1932 *J. Am. Chem. Soc.* **54** 3841
[8] Wooten F and Weaire D 1987 *Solid State Physics* vol 40 (New York: Academic) p 1
[9] Metropolis N, Rosenbluth A W, Rosenbluth M N, Teller A H and Teller E 1953 *J. Chem. Phys.* **21** 1087
[10] Keating P N 1966 *Phys. Rev.* **145** 637
[11] Leigh R S, Szigeti B and Tewary V K 1971 *Proc. R. Soc.* A **320** 505
[12] Harrison W A 1989 *Electronic Structure and the Properties of Solids* (New York: Dover)
[13] van Schilfgaarde M and Sher A 1987 *Phys. Rev.* B **36** 4375
[14] Musgrave M J P and Pople J A 1962 *Proc. R. Soc.* A **268** 474
[15] Born M and Huang K 1954 *Dynamical Theory of Crystal Lattices* (Oxford: Oxford University Press)
[16] Maradudin A A, Montroll E W, Weiss G H and Ipatova I P 1971 *Theory of Lattice Dynamics in the Harmonic Approximation (Solid State Physics Supplement 3)* 2nd edn (New York: Academic)
[17] Martin R M 1970 *Phys. Rev.* B **1** 4005
[18] Lyddane R M, Sachs R G and Teller E 1941 *Phys. Rev.* **59** 673
[19] Adachi S 1985 *J. Appl. Phys.* **58** R1
[20] Chen A B and Sher A 1981 *Phys. Rev.* B **10** 5360
[21] Martin R M 1972 *Phys. Rev.* B **5** 1607
[22] Bennett B I and Maradudin A A 1972 *Phys. Rev.* B **5** 4146
[23] Martin R M 1974 *Phys. Rev.* B **9** 1998
[24] Martin R M and Kunc K 1981 *Phys. Rev.* B **24** 2081
[25] Van Vechten J A 1977 *Inst. Phys. Conf. Ser. 31* (Bristol: Institute of Physics) p 441
[26] Seitz F and Koehler J S 1956 *Solid State Physics* vol 2 (New York: Academic) p 305
[27] Averback R S, Diaz de la Rubia T, Hsieh H and Benedek R 1991 *Nucl. Instrum. Methods* B **59/60** 709
[28] Etherington G, Wright A C, Wenzel J T, Dore J C, Clarke J H and Sinclair R N 1982 *J. Non-Cryst. Solids* **48** 265
[29] Temkin R H, Paul W and Connell G A N 1973 *Adv. Phys.* **22** 581

† We also omit ϵ_1, since the charge redistribution effects are now contained in the polarizabilities.

[30] Wooten F and Weaire D 1986 *J. Phys. C: Solid State Phys.* **19** L411
[31] Kunc K 1973-1974 *Ann. Phys., Lpz.* **8** 319
[32] Kunc K, Balkanski M and Nusimovici M A 1975 *Phys. Status Solidi* b **71** 341; 1975 *Phys. Status Solidi* b **72** 229, 249
[33] Kunc K, Balkanski M and Nusimovici M A 1975 *Phys. Rev.* B **12** 4346